Available online at www.sciencedirect.com
SCIENCE DIRECT®
International Journal of Heat and Mass Transfer 48 (2005) 37–51
International Journal of HEAT and MASS TRANSFER
www.elsevier.com/locate/ijhmt

A method for predicting heat and moisture transfer through multilayered walls based on temperature and moisture content gradients

N. Mendes [a,*], P.C. Philippi [b]

[a] Department of Mechanical Engineering, Thermal Systems Laboratory, Pontifical Catholic University of Paraná, Rua Imaculada Conceição, 1155, Curitiba, PR 80215-901, Brazil
[b] Department of Mechanical Engineering, Federal University of Santa Catarina, Florianópolis, SC 88040-900, Brazil

Received 30 September 2003; received in revised form 2 August 2004
Available online 14 October 2004

Abstract

A mathematical formulation applied to a numerically robust solver is presented, showing that moisture content gradients can be used as driving forces for heat and moisture transport calculation through the interface between porous materials with different pore size distribution functions. For comparison purposes, several boundary conditions are tested—in order to gradually increase the discontinuity effects—and a detailed analysis is undertaken for the temperature and moisture content distributions and sensible and latent heat fluxes, when the discontinuity on the moisture content profile is taken or not into account.

1. Introduction

In a given circumstance, under gradients of temperature and vapor pressure, fields of temperature and moisture content are dynamically created within building envelopes. The correct evaluation of these fields is important for accurately predicting the heat and moisture flows for thermal comfort and building energy consumption analysis. In addition, moisture can cause damage to building materials and has impact on occupants' health.

Most of the research is still carried out by using phenomenological macroscopic models, introducing heuristic laws relating thermodynamic forces to fluxes through moisture and temperature dependent transport coefficients.

In this way, one of the most disseminated and accepted macroscopic models for studying heat and moisture transfer through porous media is the Philip and De Vries model [1], which uses as driving potentials the temperature and moisture content gradients. On the other hand, it is well known that there is discontinuity on the moisture content profile at the interface between two porous media, due to their different hygroscopic behavior; material with high hygroscopicity retains more moisture at the same relative humidity and temperature. To model systems made up of dissimilar porous media, with the runabout of moisture content discontinuity problem, some authors modified the Philip and De Vries model [1] so that to use capillary pressure or relative humidity gradient instead of moisture content gradient.

* Corresponding author. Tel.: +55 41 271 1322; fax: +55 41 271 1691.
E-mail address: nathan.mendes@pucpr.br (N. Mendes).

0017-9310/$ - see front matter © 2004 Elsevier Ltd. All rights reserved.
doi:10.1016/j.ijheatmasstransfer.2004.08.011

Nomenclature

c	specific heat (J/kg K)
D_{TV}	vapor phase transport coefficient associated to a temperature gradient ($m^2/s\,K$)
$D_{\theta V}$	vapor phase transport coefficient associated to a moisture content gradient (m^2/s)
D_{TL}	liquid phase transport coefficient associated to a temperature gradient ($m^2/s\,K$)
$D_{\theta L}$	liquid phase transport coefficient associated to a moisture content gradient (m^2/s)
D_T	mass transport coefficient associated to a temperature gradient ($m^2/s\,K$)
D_θ	mass transport coefficient associated to a moisture content gradient (m^2/s)
h	heat transfer convection coefficient ($W/m^2\,K$)
h_{LV}	heat of vaporization (J/kg)
h_m	mass transfer convection coefficient (m/s)
j	total (vapor plus liquid) flow ($kg/m^2\,s$)
j_v	vapor flow ($kg/m^2\,s$)
t	time (s)
T	temperature (°C)
x	distance into the flat plate (m)
w	moisture content (kg of water/kg of porous material)

Greek symbols

λ	thermal conductivity (W/m K)
θ	total moisture volumetric content (m^3 of water/m^3 of porous material)
ρ	mass density (kg/m^3)

Subscripts

l	liquid
m	mean
o	solid matrix
v	vapor

Among these authors, it shall be cited Pedersen [2] who used the capillary suction pressure and Künzel [3] that used the relative humidity. The calculation methodology employed by them is correct since it takes this discontinuity phenomenon at the interface into account. Milly [4] (apud Janssen et al. [5]) has also reformulated the Philip and De Vries [1] equations for coupled heat and moisture transfer to obtain the porous matrix potential rather than moisture content as independent variable.

However, in many circumstances, the direct use of moisture content in some mathematical models and computer codes can be very appropriate since it can be more computationally viable and, most of time, moisture content is a more useful parameter as it has a simple and direct physical meaning. Another favorable point is that hysteresis effects may be less evident on transport coefficients associated to moisture content gradients than those associated to capillary pressure gradients. In this way, the disregard of hysteresis implies likely small errors when moisture content gradient is the driving force. In some computer codes such as UMIDUS [6] and MOIST [7], the governing equations are written in terms of temperature and moisture content. However, the MOIST code, version 3.0, changed its formulation to one based on capillary pressure gradients for considering the moisture content discontinuity at the interface between two hygroscopically dissimilar materials.

In this article, a mathematical formulation is presented to show that moisture content gradients can be used as driving forces for heat and moisture transport calculation through the interface between porous materials with different pore size distribution functions in a numerically robust way.

Nevertheless, when two materials are pressed against each other, there will be spaces filled up with air due to their rugosity, preventing perfect contact for heat flux and moisture flow. Freitas et al. [8] treated the contact resistance for moisture, with the development of the code TRHUMIDADE that needs a parameter to describe the maximum moisture flow crossing the interface, which is only obtainable by experimental means. Experimental results conducted by Qiu et al. [9] showed that a considerable hydraulic resistance could be created by the imperfect contact between two porous building materials so that the assumption of perfect hydraulic contact could lead to significant errors in predicting the moisture transport in porous building materials.

Although contact resistance can play an important role in moisture transfer through the interface between two different porous materials, consideration of contact resistance is outside the scope of this work, which is restricted to present a mathematical model that enables moisture content gradients to be used as driving forces for heat and mass transfer calculation in porous media formed by two or more dissimilar materials. The equations are also presented in an easy way to be implemented in computer codes by using the MultiTri-Diagonal-Matrix Algorithm (MTDMA) presented by Mendes and Philippi [10], which makes the model numerically stable. Results in terms of temperature and moisture content profiles, moisture flow and heat fluxes are discussed for the model presented and for a

model that does not take the discontinuity effect into account.

2. Mathematical model for the interface

Neglecting the moisture and thermal contact resistances between porous materials, it is possible to state that, at the interface between two porous media named A and B, the following equations are true:

$$\begin{cases} (T)_{\mathrm{A}} = (T)_{\mathrm{B}}, \\ (\psi)_{\mathrm{A}} = (\psi)_{\mathrm{B}}, \end{cases} \tag{1}$$

where T is the temperature and ψ the capillary pressure.

According to Kelvin's law and the equality $(\psi)_{\mathrm{A}} = (\psi)_{\mathrm{B}}$, it is possible to write

$$\frac{\Re(T)_{\mathrm{A}}}{Mg}\ln(\phi)_{\mathrm{A}} = \frac{\Re(T)_{\mathrm{B}}}{Mg}\ln(\phi)_{\mathrm{B}}, \tag{2}$$

where $\Re$ is the universal constant for gases, M, the molecular mass, ϕ the relative humidity and g the gravity. Since the temperatures for both materials can be considered to be the same at the interface, Eq. (2) turns into

$$(\phi)_{\mathrm{A}} = (\phi)_{\mathrm{B}}, \tag{3}$$

which means that the relative humidity is the same.

Therefore, the vapor concentration—ρ_{v}—is also the same and as an ideal gas it can be written as

$$\rho_{\mathrm{v}}(s) = \frac{P_{\mathrm{S}}(s)}{T(s)}\frac{\phi(s)M}{\Re}, \tag{4}$$

where s represents the interface between the two materials.

On the other hand, the quotient between saturation pressure—P_{S}—and temperature can be written as a polynomial function in terms of temperature. This quotient P_{S}/T can be still expressed as a temperature linear function with small error for a certain range of temperature, as shown in Fig. 1.

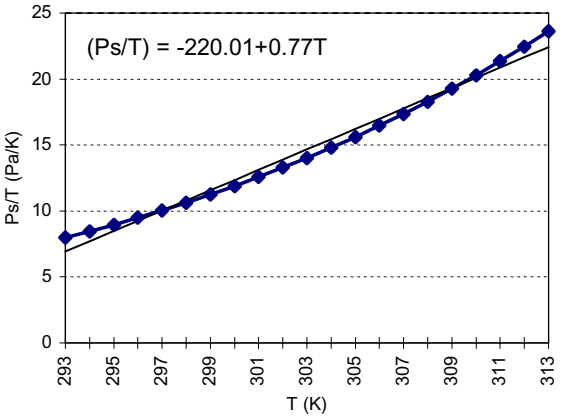

Fig. 1. Linearization of $\frac{P_{\mathrm{S}}}{T} = f(T)$.

$$R(T) = \frac{P_{\mathrm{S}}}{T} - (AT + B), \tag{5}$$

for correcting P_{S} at each iteration. In Eq. (5), A and B are the angular and linear coefficients of the straight line $P_{\mathrm{S}}/T = AT + B$. The first left-hand term, P_{S}/T, is calculated from the saturation pressure correlation, which is only dependent on the temperature.

Therefore, from,

$$\frac{P_{\mathrm{S}}}{T} = R(T) + (AT + B). \tag{6}$$

Eq. (4) can be expressed as

$$\rho_{\mathrm{v}}(s) = \frac{(R(T) + (AT + B))\phi(s)M}{\Re}. \tag{7}$$

Additionally, the sorption/desorption curve, provides a one-to-one relationship with the relative humidity, so that when truncating the Taylor series after the second-order term, the following is obtained:

$$\phi(s) = \phi(s)^{\mathrm{prev}} + \left(\frac{\partial\phi}{\partial\theta}\right)^{\mathrm{prev}}(\theta(s) - \theta(s)^{\mathrm{prev}}), \tag{8}$$

where $\theta(s)^{\mathrm{prev}}$ is the volumetric moisture content calculated at the previous iteration.

Thereupon, replacing the relative humidity, the vapor concentration (Eq. (7)) can be now written as

$$\rho_{\mathrm{v}}(s) = \frac{\left(R(T)\phi(s)^{\mathrm{prev}} + (AT + B)\phi(s)^{\mathrm{prev}} + \left(\frac{P_{\mathrm{S}}(s)}{T(s)}\right)^{\mathrm{prev}}\left(\frac{\partial\phi}{\partial\theta}\right)^{\mathrm{prev}}(\theta(s) - \theta(s)^{\mathrm{prev}})\right)M}{\Re}. \tag{9}$$

In order to reach a higher accuracy degree when a linear expression is used, a residual function $R(T)$ is introduced as

Consequently, as the vapor concentrations at both interface sides (materials A and B) are the same, the following equality can be written:

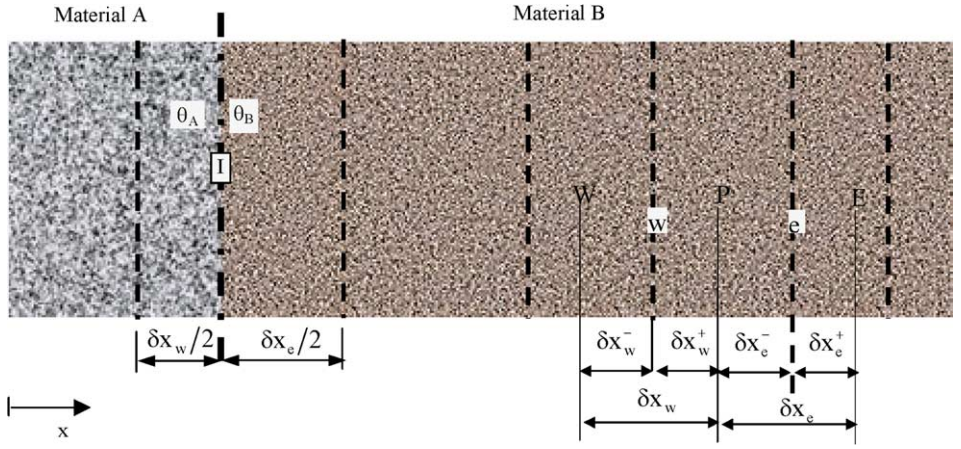

Fig. 2. Schematic representations for a control volume at the interface between two porous media and for the generic discretization between west (W) and east (E) boundaries.

$$\left(\frac{\partial\phi}{\partial\theta}\right)_{\mathrm{A}}^{\mathrm{prev}}(\theta_{\mathrm{A}}(s)-\theta_{\mathrm{A}}(s)^{\mathrm{prev}}) = \left(\frac{\partial\phi}{\partial\theta}\right)_{\mathrm{B}}^{\mathrm{prev}}(\theta_{\mathrm{B}}(s)-\theta_{\mathrm{B}}(s)^{\mathrm{prev}}), \tag{10}$$

which no longer depends on the temperature for a given time.

Eq. (10) can also be written in a shorter way as

$$\theta_{\mathrm{B}}(s) = C_1\theta_{\mathrm{A}}(s) + C_2, \tag{11}$$

where

$$C_1 = \frac{\left(\frac{\partial\phi}{\partial\theta}\right)_{\mathrm{A}}^{\mathrm{prev}}}{\left(\frac{\partial\phi}{\partial\theta}\right)_{\mathrm{B}}^{\mathrm{prev}}} \tag{12}$$

and

$$C_2 = \theta_{\mathrm{B}}^{\mathrm{prev}} - C_1\theta_{\mathrm{A}}^{\mathrm{prev}}. \tag{13}$$

On the other hand, analyzing the control volume at the interface I shown in Fig. 2, one can calculate spatially averaged moisture content as

$$\theta_I = \frac{\delta x_{\mathrm{w}}}{\delta x_{\mathrm{w}}+\delta x_{\mathrm{e}}}\theta_{\mathrm{A}} + \frac{\delta x_{\mathrm{e}}}{\delta x_{\mathrm{w}}+\delta x_{\mathrm{e}}}\theta_{\mathrm{B}}, \tag{14}$$

where δx_{e} and δx_{w} represent the distances between the interface and the east and west boundaries of the control volume I, as shown in Fig. 2.

In Section 3, the mass and energy conservation equations are presented so that the formulation described above for the discontinuity on the moisture content profile is included in the governing equations.

3. General governing equations

The porous medium to be modeled is assumed to be non-deformable and free of chemical reactions. The moist air mass density is taken to be constant. In addition, restricting the analysis to low air permeability and low porosity materials, viscous forces are much more important than the buoyant ones so that convective moisture transfer effects can be neglected.

Thus, the governing partial differential equations in a porous media are derived from the conservation laws of both mass and energy applied to an elemental control volume. For the mass conservation equation, the presence of both liquid and vapor phases was considered.

3.1. Mass conservation equation

Using Philip and De Vries [1] phenomenological model and neglecting the gravity term, the mass conservation equation can be written in a volumetric basis as

$$\frac{\partial\theta}{\partial t} = \nabla\cdot(D_\theta\nabla\theta_{\mathrm{l}}) + \nabla\cdot(D_{\mathrm{T}}\nabla T) \tag{15}$$

with $D_{\mathrm{T}} = D_{\mathrm{TL}} + D_{\mathrm{TV}}$ and $D_\theta = D_{\theta\mathrm{L}} + D_{\theta\mathrm{V}}$, where D_{TL} is the liquid phase transport coefficient associated to a temperature gradient, D_{TV}, vapor phase transport coefficient associated to a temperature gradient, $D_{\theta\mathrm{L}}$, liquid phase transport coefficient associated to a moisture content gradient, $D_{\theta\mathrm{V}}$, vapor phase transport coefficient associated to a moisture content gradient, D_{T}, mass transport coefficient associated to a temperature gradient ($\mathrm{m^2/s\,K}$) and D_θ, mass transport coefficient associated to a moisture content gradient ($\mathrm{m^2/s}$).

When moisture content is high, capillary migration takes place rather than diffusion what substantially increases the moisture flow through the porous structure. On the other hand, when the porous medium moisture content is low, vapor migration is predominant. This predominance is mathematically represented by the coefficients $D_{\theta\mathrm{V}}$ and $D_{\theta\mathrm{L}}$, which are associated to moisture content gradients.

Since the main gradients for both temperature and moisture content are on the x-axis direction (which crosses the building element from outside to inside), the 1-D modeling hypothesis is considered. Thus, at the interface, the continuity equation is written as

$$\frac{\partial \theta_I}{\partial t} = \frac{\partial}{\partial x}\left(D_\theta \frac{\partial \theta}{\partial x} + D_T \frac{\partial T}{\partial x}\right), \tag{16}$$

where the transient term of moisture content at the interface, given by Eq. (14), can be discretized in an implicit way as

$$\frac{\partial \theta_I}{\partial t} = \frac{\delta x_w}{\delta x_w + \delta x_e}\frac{\theta_A(s) - \theta_A^0(s)}{\Delta t} + \frac{\delta x_e}{\delta x_w + \delta x_e}\frac{\theta_B(s) - \theta_B^0(s)}{\Delta t} \tag{17}$$

or, just in terms of θ_A as

$$\begin{aligned}\frac{\partial \theta_I}{\partial t} = {} & \frac{1}{\Delta t}\left(\frac{\delta x_w}{\delta x_w + \delta x_e} + \frac{\delta x_e}{\delta x_w + \delta x_e}C_1\right)\theta_A(s) \\ & + \frac{1}{\Delta t}\left(\frac{\delta x_e}{\delta x_w + \delta x_e}C_2\right) - \frac{1}{\Delta t}\left(\frac{\delta x_w}{\delta x_w + \delta x_e}\right)\theta_A^0(s) \\ & - \frac{1}{\Delta t}\left(\frac{\delta x_e}{\delta x_w + \delta x_e}\right)\theta_B^0(s).\end{aligned} \tag{18}$$

Using a central difference scheme (CDS) and neglecting the gravity term in the moisture flow at west and east boundaries, the mass conservation equation can be generically presented as

$$\begin{aligned}& \left[\frac{\Delta x}{\Delta t}\left(\frac{\delta x_w}{\delta x_w + \delta x_e} + \frac{\delta x_e}{\delta x_w + \delta x_e}C_1\right) + \frac{D_{\theta e}}{\delta x_e}C_1 + \frac{D_{\theta w}}{\delta x_w}\right]\theta_{P-}(s) \\ & \quad + \left(\frac{D_{Tw}}{\delta x_w} + \frac{D_{Te}}{\delta x_e}\right)T_p \\ & \quad = \frac{D_{\theta e}}{\delta x_e}\theta_E + \frac{D_{\theta w}}{\delta x_w}\theta_W + \frac{D_{Te}}{\delta x_e}T_E + \frac{D_{Tw}}{\delta x_w}T_W \\ & \qquad - \frac{\Delta x}{\Delta t}\left(\frac{\delta x_e}{\delta x_w + \delta x_e}C_2\right) + \frac{\Delta x}{\Delta t}\left(\frac{\delta x_w}{\delta x_w + \delta x_e}\right)\theta_{P-}^0(s) \\ & \qquad + \frac{\Delta x}{\Delta t}\left(\frac{\delta x_e}{\delta x_w + \delta x_e}\right)\theta_{P+}^0(s) - \frac{D_{\theta e}}{\delta x_e}C_2,\end{aligned} \tag{19}$$

where the moisture content at the right and left sides of the interface are respectively

$$\begin{aligned}\theta_{P-}(s) &= \theta_A(s), \\ \theta_{P+}(s) &= \theta_B(s).\end{aligned} \tag{20}$$

3.2. Energy conservation equation

An energy balance in an elemental control volume of porous material, disregarding heat transfer by convection and by radiation, leads to the following energy conservation equation:

$$\frac{\partial}{\partial t}[\rho_0(h_s + h_l w_l + h_v w_v)] = -\nabla \cdot (\mathbf{q} + h_l \mathbf{j}_l + h_v \mathbf{j}_v). \tag{21}$$

However, if (i) the vapor mass is considered to be much lower than the liquid mass, (ii) the sensible heat transfer that occurs in both liquid ($c_l j_l \nabla T$) and vapor ($c_v j_v \nabla T$) phases is negligible, (iii) the water vapor is classified as a perfect gas due to the low vapor partial pressure and (iv) the Kelvin's law is applied, the energy conservation equation can be reduced to

$$\rho_0 c_m \frac{\partial T}{\partial t} = -\nabla \cdot \mathbf{q} - L\nabla \cdot \mathbf{j}_v, \tag{22}$$

where j_v is the vapor flow from the Philip and De Vries model [1].

The second right-hand term gives the distillation effects induced by both temperature and moisture content gradients. In some applications where those gradients are moderate, that term can be disregarded. However, at the interface between two different porous materials this term can play an important role on the energy rate calculation.

Similarly to what was done for the mass conservation equation, the 1-D hypothesis is also considered, which gives

$$\rho_0 \cdot c_m \cdot \frac{\partial T}{\partial t} = -\nabla q - L \cdot \nabla j_v \tag{23}$$

or

$$\begin{aligned}\rho_0 c_m(\theta)\frac{\partial T}{\partial t} = {} & \frac{\partial}{\partial x}\left(\lambda(\theta, T)\frac{\partial T}{\partial x}\right) \\ & + L(T)\rho_l \frac{\partial}{\partial x}\left(D_{TV}(\theta, T)\frac{\partial T}{\partial x} + D_{\theta V}(\theta, T)\frac{\partial \theta}{\partial x}\right).\end{aligned} \tag{24}$$

Analogously, using the interface condition, the following can be written for the energy conservation equation:

$$\begin{aligned}& \left(L\rho_l \frac{D_{\theta Ve}}{\delta x_e}C_1 + L\rho_l \frac{D_{\theta Vw}}{\delta x_w}\right)\theta_{P-} \\ & \quad + \left(\rho_0 c_m \frac{\Delta x}{\Delta t} + \frac{\lambda_e}{\delta x_e} + \frac{L\rho_l D_{TVe}}{\delta x_e} + \frac{\lambda_w}{\delta x_w} + \frac{L\rho_l D_{TVw}}{\delta x_w}\right)T_P \\ & \quad = L\rho_l \frac{D_{\theta Ve}}{\delta x_e}\theta_E + L\rho_l \frac{D_{\theta Vw}}{\delta x_w}\theta_W + \left(\frac{\lambda_e}{\delta x_e} + \frac{L\rho_l D_{TVe}}{\delta x_e}\right)T_E \\ & \qquad + \left(\frac{\lambda_w}{\delta x_w} + \frac{L\rho_l D_{TVw}}{\delta x_w}\right)T_W + \rho_0 c_m \frac{\Delta x}{\Delta t}T_P^0 - L\rho_l \frac{D_{\theta Ve}}{\delta x_e}C_2.\end{aligned} \tag{25}$$

Therefore, Eq. (25) is written considering the temperature and the moisture content in a separate way so that they can be simultaneously calculated by using the algorithm presented by Mendes and Philippi [10].

4. Solution procedure

The discretization procedure is the same described in Patankar [11]. In Fig. 2, the nodes are presented according to Patankar's nomenclature. The transport coefficients are calculated over the interfaces between two control volumes. To represent in a better way the fluxes through two consecutive elements, a harmonic mean was introduced and for a given coefficient D, it can be written as

$$\frac{\delta x_e}{D_e} = \frac{\delta x_e^-}{D_P} + \frac{\delta x_e^+}{D_E}, \tag{26}$$

where δx_e^- *e* δx_e^+ represent the distances shown in Fig. 2.

For a uniform grid, the transport coefficients are calculated over the interfaces e and w, as

$$D_e = \frac{2}{\frac{1}{D_P} + \frac{1}{D_E}} \quad \text{and} \quad D_w = \frac{2}{\frac{1}{D_P} + \frac{1}{D_W}}. \tag{27}$$

For the solution of the combined governing equations, the MTDMA algorithm, presented by Mendes and Philippi [10], is proposed here to solve all the governing equations in a simultaneous way.

Then, the discretization of the heat and mass transfer coupled equations have to be done in the following form:

$$\mathbf{A_i} \cdot \mathbf{x_i} = \mathbf{B_i} \cdot \mathbf{x_{i+1}} + \mathbf{C_i} \cdot \mathbf{x_{i-1}} + \mathbf{D_i}, \tag{28}$$

where x is a vector containing the m dependent variables; in this case θ and T.

Due to the great complexity of the process and to the lack of information on the interface between two porous materials, it is admitted hydraulic continuity, i.e., additional resistance to moisture flow is not created at the interface; in addition, the interface is placed right in the middle of the control volume. Actually, when hydraulic discontinuity is disregarded, the model seems to be more accurate when vapor transport is dominant.

On the other hand, temperature gradients may affect moisture flow more significantly when the Posnov number is high [12] and the thermal contact resistance may play a more important role on the moisture flow across the interface when no perfect contact is considered. The Posnov number is defined as $Pn = \frac{D_T \Delta T}{D_\theta \eta}$, where ΔT is the characteristic temperature difference and η is the porosity. This number reports the importance of temperature gradients on the moisture transport through porous materials. Consequently, for high Posnov numbers, the moisture transport occurs predominantly due to temperature gradients. Therefore, this dimensionless number significance arises when $\frac{\partial \theta}{\partial x} \to 0$.

As perfect contact is considered in the present model, the transport coefficients are evaluated at the interface by harmonic means between two consecutive grid elements; this assures that they are evaluated in the same material. However, the thermal capacity is calculated by summing the capacities of both materials that form the interface control volume.

Therefore, for interface node I, the following coefficients can be written for the MTDMA:

$$A(I) = \begin{bmatrix} \frac{\Delta x}{\Delta t}\left(\frac{\delta x_w}{\delta x_w + \delta x_e} + \frac{\delta x_e}{\delta x_w + \delta x_e} C_1\right) + \frac{D_{\theta e}}{\delta x_e} C_1 + \frac{D_{\theta w}}{\delta x_w} & \frac{D_{Te}}{\delta x_e} + \frac{D_{Tw}}{\delta x_w} \\ L\rho_l\left(\frac{D_{\theta Ve}}{\delta x_e} C_1 + \frac{D_{\theta Vw}}{\delta x_w}\right) & \left(\frac{\lambda_e}{\delta x_e} + \frac{L\rho_l D_{TVe}}{\delta x_e} + \frac{\lambda_w}{\delta x_w} + \frac{L\rho_l D_{TVw}}{\delta x_w} + \rho_0 c_m \frac{\Delta x}{\Delta t}\right) \end{bmatrix};$$

$$B(I) = \begin{bmatrix} \frac{D_{\theta e}}{\delta x_e} & \frac{D_{Te}}{\delta x_e} \\ L\rho_l \frac{D_{\theta Ve}}{\delta x_e} & \left(\frac{\lambda_e}{\delta x_e} + \frac{L\rho_l D_{TVe}}{\delta x_e}\right) \end{bmatrix}; \quad C(I) = \begin{bmatrix} \frac{D_{\theta w}}{\delta x_w} & \frac{D_{Tw}}{\delta x_w} \\ L\rho_l \frac{D_{\theta Vw}}{\delta x_w} & \left(\frac{\lambda_w}{\delta x_w} + \frac{L\rho_l D_{TVw}}{\delta x_w}\right) \end{bmatrix}; \tag{29}$$

$$D(I) = \begin{bmatrix} \frac{\Delta x}{\Delta t}\left(\frac{\delta x_w}{\delta x_w + \delta x_e}\right)\theta^0_{P-}(s) + \frac{\Delta x}{\Delta t}\left(\frac{\delta x_e}{\delta x_w + \delta x_e}\right)\theta^0_{P+}(s) - \frac{\Delta x}{\Delta t}\left(\frac{\delta x_e}{\delta x_w + \delta x_e} C_2\right) - \frac{D_{\theta e}}{\delta x_e} C_2 \\ \rho_0 c_m \frac{\Delta x}{\Delta t} T^0_P - L\rho_l \frac{D_{\theta Ve}}{\delta x_e} C_2 \end{bmatrix}.$$

In Eq. (28), coefficients A, B and C are second-order tensors, in which each line corresponds to one dependent variable. The elements that do not belong to the main diagonal are the coupled terms for each conservation equation.

Per contra, the neighbor node at the interface right-hand side should be also modified so that the moisture content gradient be referred to the value associated to material B—$\theta_{P+}(I) = \theta_B$—and no longer to material A. Hence, the coefficients can be generically and grid-inde-

pendently written for any internal node of the physical domain as

$$A(I)=\begin{bmatrix}\dfrac{\Delta x}{\Delta t}\left(\dfrac{\delta x_w}{\delta x_w+\delta x_e}+\dfrac{\delta x_e}{\delta x_w+\delta x_e}C_1\right)+\dfrac{D_{\theta e}}{\delta x_e}C_1+\dfrac{D_{\theta w}}{\delta x_w} & \dfrac{D_{Te}}{\delta x_e}+\dfrac{D_{Tw}}{\delta x_w}\\ L\rho_l\left(\dfrac{D_{\theta Ve}}{\delta x_e}C_1+\dfrac{D_{\theta Vw}}{\delta x_w}\right) & \left(\dfrac{\lambda_e}{\delta x_e}+\dfrac{L\rho_l D_{TVe}}{\delta x_e}+\dfrac{\lambda_w}{\delta x_w}+\dfrac{L\rho_l D_{TVw}}{\delta x_w}+\rho_0 c_m\dfrac{\Delta x}{\Delta t}\right)\end{bmatrix};$$

$$B(I)=\begin{bmatrix}\dfrac{D_{\theta e}}{\delta x_e} & \dfrac{D_{Te}}{\delta x_e}\\ L\rho_l\dfrac{D_{\theta Ve}}{\delta x_e} & \left(\dfrac{\lambda_e}{\delta x_e}+\dfrac{L\rho_l D_{TVe}}{\delta x_e}\right)\end{bmatrix};\quad C(I)=\begin{bmatrix}\dfrac{D_{\theta w}}{\delta x_w}C_3 & \dfrac{D_{Tw}}{\delta x_w}\\ L\rho_l\dfrac{D_{\theta Vw}}{\delta x_w}C_3 & \left(\dfrac{\lambda_w}{\delta x_w}+\dfrac{L\rho_l D_{TVw}}{\delta x_w}\right)\end{bmatrix};\tag{30}$$

$$D(I)=\begin{bmatrix}\dfrac{\Delta x}{\Delta t}\left(\dfrac{\delta x_w}{\delta x_w+\delta x_e}\right)\theta^0_{P-}(s)+\dfrac{\Delta x}{\Delta t}\left(\dfrac{\delta x_e}{\delta x_w+\delta x_e}\right)\theta^0_{P+}(s)-\dfrac{\Delta x}{\Delta t}\left(\dfrac{\delta x_e}{\delta x_w+\delta x_e}C_2\right)-\dfrac{D_{\theta e}}{\delta x_e}C_2+\dfrac{D_{\theta w}}{\delta x_w}C_4\\ \rho_0 c_m\dfrac{\Delta x}{\Delta t}T^0_P-L\rho_l\left(\dfrac{D_{\theta Ve}}{\delta x_e}C_2+\dfrac{D_{\theta Vw}}{\delta x_w}C_4\right)\end{bmatrix}.$$

Thus, to make the algorithm computationally functional, the coefficients C_1 and C_2 should be calculated and the following cases have to be reminded: (i) for the interface node, do $C_3 = 1$ and $C_4 = 0$; (ii) if the node comes right after the interface one, do: $C_3 = C_1$ and $C_4 = C_2$. However, do $C_1 = 1$ and $C_2 = 0$; (iii) else, for any other internal node, do $C_1 = C_3 = 1$ and $C_2 = C_4 = 0$.

4.1. Boundary conditions

At the external free surfaces, the wall material is exposed to convection heat and mass transfers and phase change so that the boundary condition energy conservation equation can be written as

$$-\left(\lambda(T,\theta)\frac{\partial T}{\partial x}\right)_S-(L(T)j_v)_S=h(T_\infty-T_S)+L(T)h_m(\rho_{v,\infty}-\rho_{v,S}),\tag{31}$$

where the term $h(T_\infty - T_S)$ represents the heat exchanged with the outside air, described by the surface conductance h and $h_m(\rho_{v,\infty} - \rho_{v,S})$, the phase change energy term. The mass convection coefficient is defined as h_m and it is related to h by the Lewis' relation.

In the same way, the mass balance at the surface can be described by the following expression:

$$-\frac{\partial}{\partial x}\left(D_\theta(T,\theta)\frac{\partial\theta}{\partial x}+D_T(T,\theta)\frac{\partial T}{\partial x}\right)_S=\frac{h_m}{\rho_l}(\rho_{v,\infty}-\rho_{V,S}).\tag{32}$$

The vapor concentration difference, $\Delta\rho_v$, Eqs. (31) and (32), is normally determined by using the values of previous iterations for temperature and moisture content, generating numerical instability problems. Due to the numerical instability created by this source term, the solution of the linear set of discretized equations normally requires the use of very small time steps, which can be exceedingly time consuming, especially in long-term simulations.

In order to raise the simulation time step, Mendes et al. [13] presented a mathematical procedure to calculate the vapor flow, independently of previous values of temperature and moisture content. In this way, the term $(\Delta\rho_v)$ was linearized as a linear combination of temperature and moisture content, viz.,

$$(\rho_{v,\infty}-\rho_v(s))=M_1(T_\infty-T(s))+M_2(\theta_\infty-\theta(s))+M_3,\tag{33}$$

where

$$M_1=A\frac{M}{\Re}\phi,$$

$$M_2=\frac{M}{\Re}\left(\frac{P_S(s)}{T(s)}\right)^{prev}\left(\frac{\partial\phi}{\partial\theta(s)}\right)^{prev},$$

$$M_3=\frac{M}{\Re}\left[\left(\frac{P_S(s)}{T(s)}\right)^{prev}R(\theta^{prev}(s))+\phi_\infty(R(T_\infty)-R(T^{prev}(s)))\right].$$

Therefore, for the boundary volume S, replacing Eq. (33) into Eqs. (31) and (32) and writing the equations to be applied to MTDMA, the following coefficients are obtained:

$$A(s) = \begin{bmatrix} \dfrac{\Delta x}{2\Delta t} + \dfrac{D_{\theta e}}{\delta x_e} + M_2 \dfrac{h_m}{\rho_l} & \dfrac{D_{Te}}{\delta x_e} + M_1 \dfrac{h_m}{\rho_l} \\ \dfrac{L\rho_l D_{\theta Ve}}{\delta x_e} + LM_2 h_m & \rho_0 c_m \dfrac{\Delta x}{2\Delta t} + \dfrac{\lambda_e}{\delta x_e} + \dfrac{L\rho_l D_{TVe}}{\delta x_e} + h + LM_1 h_m \end{bmatrix};$$

$$B(s) = \begin{bmatrix} \dfrac{D_{\theta e}}{\delta x_e} & \dfrac{D_{Te}}{\delta x_e} \\ \dfrac{L\rho_l D_{\theta Ve}}{\delta x_e} & \left(\dfrac{\lambda_e}{\delta x_e} + \dfrac{L\rho_l D_{TVe}}{\delta x_e} \right) \end{bmatrix}; \quad C(s) = \begin{bmatrix} 0 & 0 \\ 0 & 0 \end{bmatrix}; \tag{34}$$

$$D(S) = \begin{bmatrix} \dfrac{h_m}{\rho_l}(M_1 T_\infty + M_2 \theta_\infty + M_3) + \dfrac{\Delta x}{2\Delta t}\theta^0(S) \\ hT_\infty + Lh_m(M_1 T_\infty + M_2 \theta_\infty + M_3) + \rho_0 c_m \dfrac{\Delta x}{2\Delta t} T^0(S) \end{bmatrix}.$$

5. Results

In order to verify the model presented in this article, a *C* code was written, allowing to compare the results when the discontinuity phenomenon on moisture content profile is taken or not into account. The case study was a porous flat wall formed by 3 layers: 2 cm of mortar, 10 cm of brick and 2 cm of mortar. Fig. 3 shows schematically this physical model. The properties used for these materials were obtained by Perrin [14], allowing all transport coefficients to be modeled as a function of moisture content. Considering the temperature range of interest in building applications, temperature dependence was neglected when compared to their dependence with moisture content. Sorption isotherms were also taken from Perrin [14], however an average curve between adsorption and desorption curves was used since hysteresis is not taken into account.

The boundary conditions for the external surfaces were those of Robin for both energy and mass conservation equations.

In the sub-sections below, the boundary conditions are gradually changed so that higher differences can be noticed on the results when the discontinuity is taken or not into account. In Section 5.1, simulations are performed using constant boundary conditions, then sinusoidal functions in Section 5.2 and, to conclude, in Section 5.3, rain effects are added so that discontinuity effects are gradually increased in terms of moisture content and temperature distributions and heat fluxes.

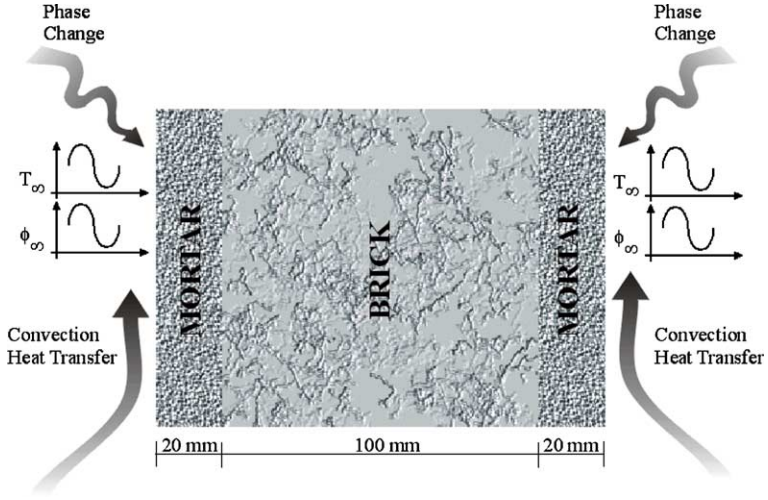

Fig. 3. Schematic representation for the physical model.

5.1. Using constant conditions for air temperature and relative humidity

In Figs. 4 and 5, the air temperature, the air relative humidity and the convection heat transfer coefficient are assumed to be constant and equal to 35 °C, 60% and 5 W/m^2K, respectively, while the initial conditions are considered equal to 20 °C and 0.05% vol. for, respectively, temperature and moisture content.

Fig. 4 shows the evolution of moisture content at the left side, $(s)-$, and right side, $(s)+$, of the interface mortar/brick, contrasting them with the interface moisture content calculated using a model that neglects the discontinuity effect between both materials (Theta (continuous)). By neglecting this effect, the tendency of the interface moisture content to be in between the values calculated for the right and left sides is noticed.

Fig. 5 shows the profiles of moisture content after 300 h. In this case, the discontinuity can be easily pointed out and noted that higher inaccuracies on the determination of moisture content can take place if the profile discontinuity is disregarded.

On the other hand, despite thermal conductivity and vapor transport coefficients are moisture-dependent, no significant differences were noticed (not shown) on the temperature profiles calculated by both ways. This can be explained by the fact that moisture content for the non-discontinuity case is approximately the average between θ_A and θ_B, which does not impact on the energy balance using the model with discontinuity on the moisture content profile.

5.2. Using sinusoidal functions for external and internal air

In order to test the models under time variable boundary conditions, sinusoidal functions are introduced for temperature and for relative humidity as illustrated in

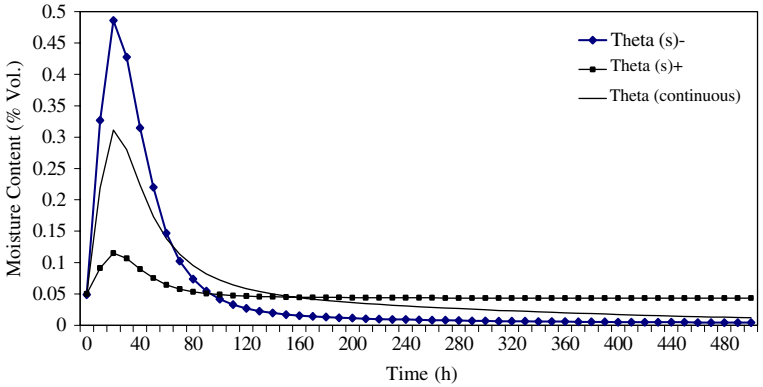

Fig. 4. Evolution of moisture content at the interface mortar/brick using constant boundary conditions.

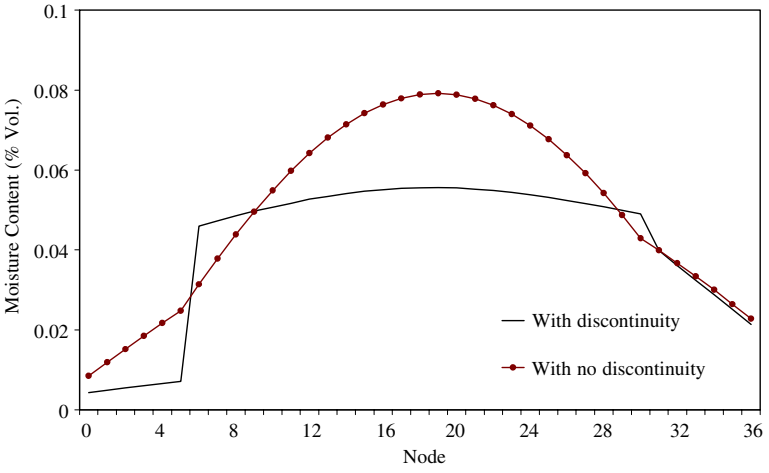

Fig. 5. Profiles of moisture content at $t = 300$ h using constant boundary conditions.

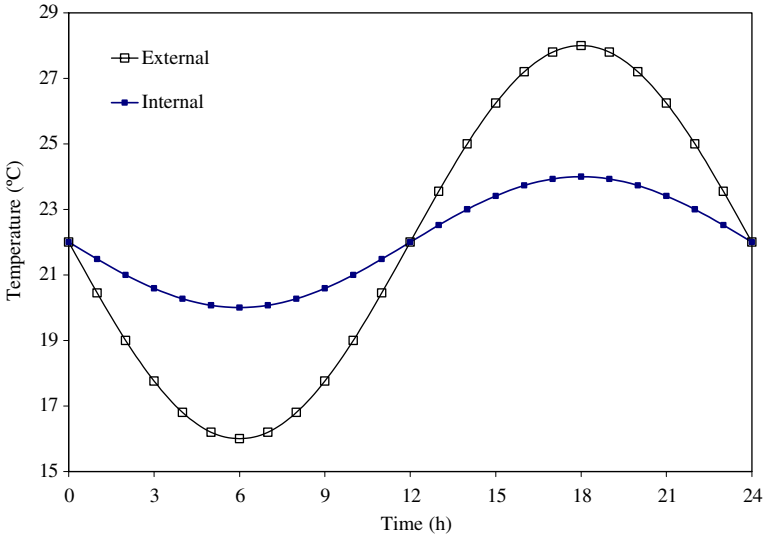

Fig. 6. Sinusoidal functions for external and internal temperatures.

Figs. 6 and 7. In the results obtained in Figs. 8–12, the initial wall temperature was considered to be 20 °C and the moisture content 0.0005 m^3/m^3 along the whole thickness.

Fig. 8 shows the evolution of moisture content profiles for the two models. For the model that does not consider the discontinuity effects on the moisture content profile, an overestimation is found that can be predominantly characterized as a physical adsorption process. The highest error found between the values presented in Fig. 8 was 641% at $t = 48$ h and, in average, it was 15%. However, at the two boundaries, the moisture content magnitudes, calculated by both models, are nearly the same, which prevents high differences on the temperature profile due to the very low difference in the phase change term of the boundary condition equation. This effect can be seen on the temperature profiles shown in Fig. 9.

However, the moisture content profile is progressively modified and the distortions start to be more evident, with higher influence on the temperature, as presented in Fig. 10 with the internal surface temperature evolution. For the first 230 h, the internal surface temperature does not visually change, however for a

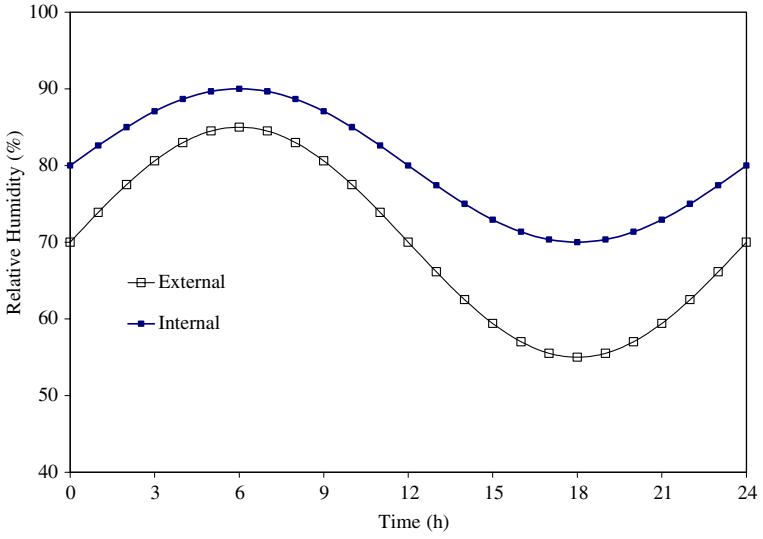

Fig. 7. Sinusoidal functions for internal and external relative humidity.

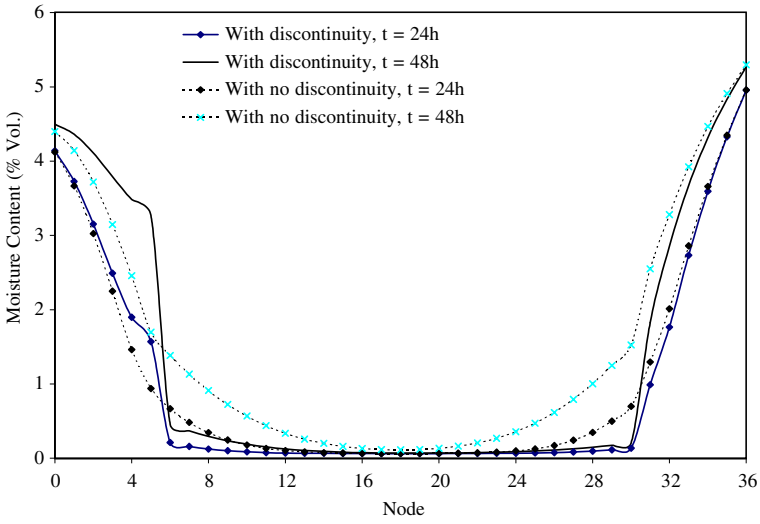

Fig. 8. Moisture content profiles using sinusoidal functions for internal and external air.

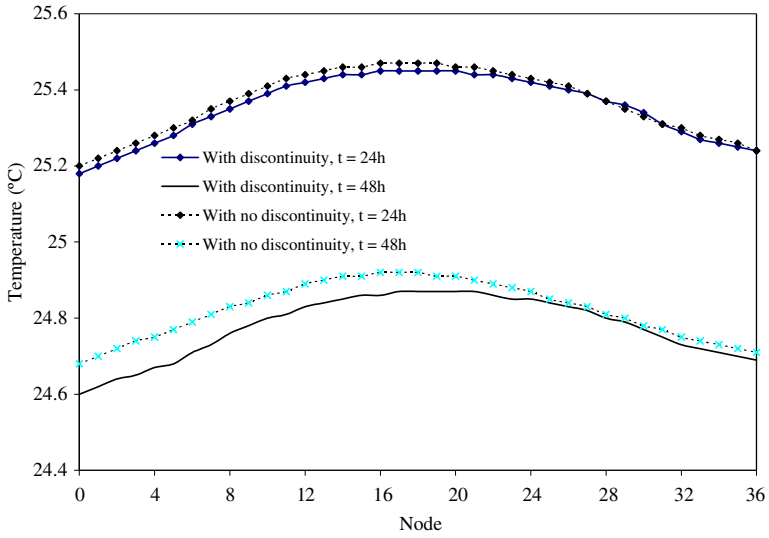

Fig. 9. Temperature profiles using sinusoidal functions for internal and external air.

longer period, higher differences can be found, which can be explained by the moisture content profiles illustrated in Fig. 11, where the discontinuity influence can be greatly noticed. This case shows the remarkable importance of the material hygroscopicity on the building conduction loads and on the strategies to avoid interstitial condensation when considering, e.g., a less hygroscopic material in the central part of a building envelope.

Fig. 12 shows the sensible and latent heat fluxes for the two models during the first 50 h. For this period, there is no perceivable difference since the moisture content profile did not play any important role on the energy balance.

Mendes et al. [15] showed that for predicting conduction loads, some simplifications on the Philip and De Vries [1] model such as the omission of the phase change term on the energy conservation equation could be reasonably made in nodes that are not at the boundaries. In fact, when water, released by evaporation, leaves a pore or a liquid island, the vapor diffuses through the medium until it encounters a small cavity or liquid island, where it condenses, releasing energy by phase change. As a result, the heat balance is more or less unchanged since the

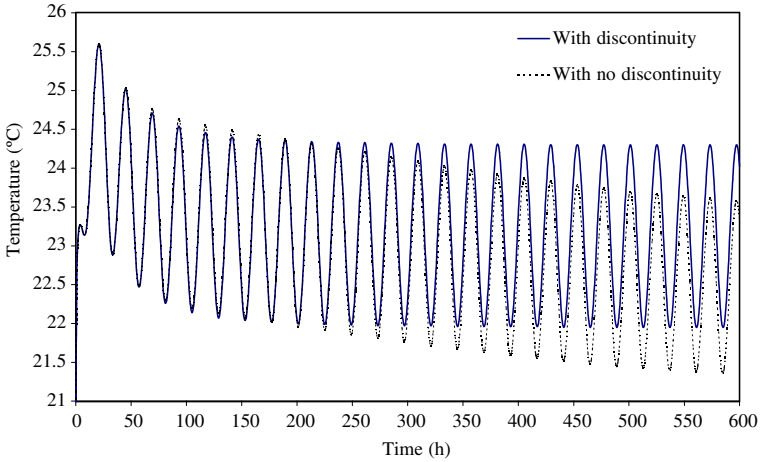

Fig. 10. Internal surface temperature evolution using sinusoidal functions for internal and external air.

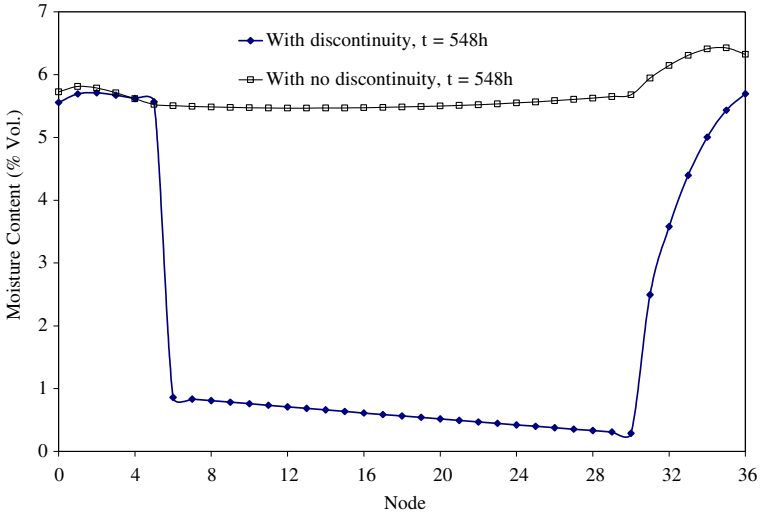

Fig. 11. Moisture content profile at $t = 548$ h using sinusoidal functions for internal and external air.

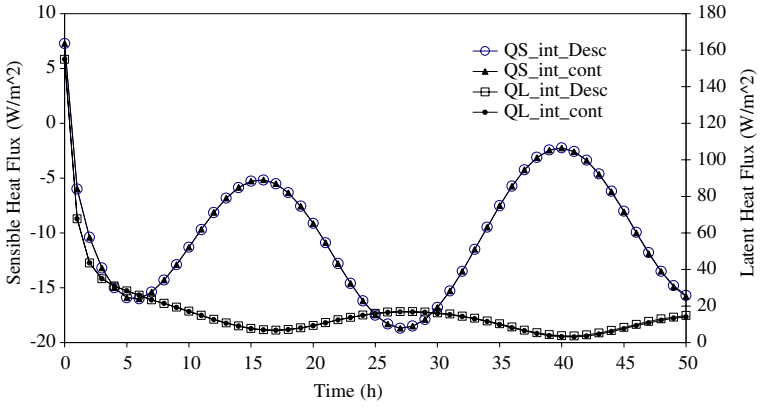

Fig. 12. Sensible and latent heat fluxes during the first 50 h using sinusoidal functions for internal and external air.

evaporated and condensed portions are roughly equal. On the other hand, the computer run time may be reduced up to 37%, which can be greatly appreciated in yearly building hygrothermal simulations.

Nevertheless, this phase change term and the moisture content profile discontinuity effect might be much more meaningful under circumstances where higher gradients of moisture content are present. Santos and Mendes [16] have analyzed the problem concerning the evolution of an imbibition front and noticed that the phase change term may become greater than the heat diffusion term.

In this way, rain effects were also considered (Section 5.3) so that moisture content gradients impact more substantially on the temperature profile via the phase change term on the set of energy conservation equations.

5.3. Using sinusoidal functions for external and internal air and rain at the external side of the wall

As temperature profiles are rather moisture-dependent than temperature-dependent when high gradients of moisture content are present, a Dirichlet condition was considered for moisture content at the external side of the wall, representing the rain effects. Then, this rain boundary condition was set so that the external wall surface was fully saturated of water, i.e., the moisture content was considered to be equal to the lime mortar porosity (18%).

In this case, which results are shown in Figs. 13–15, the initial moisture content was based on a 60% relative humidity for the three layers of the wall presented in Fig. 3.

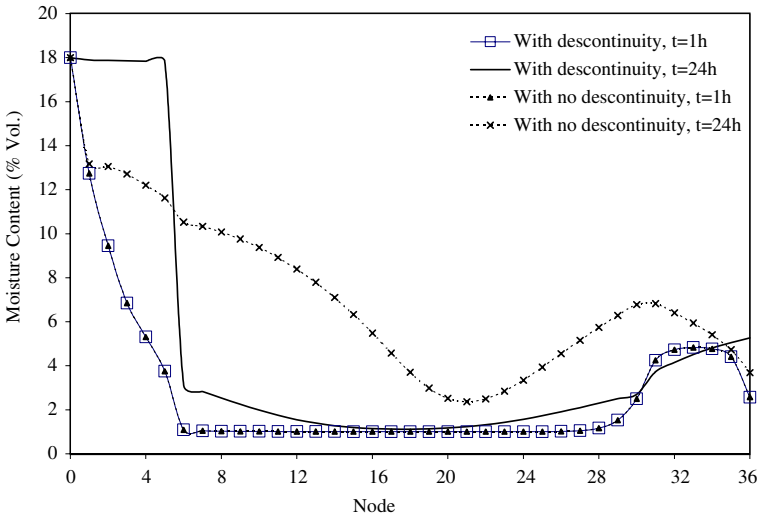

Fig. 13. Moisture content profile at 1 h and 24 h under the rain boundary condition.

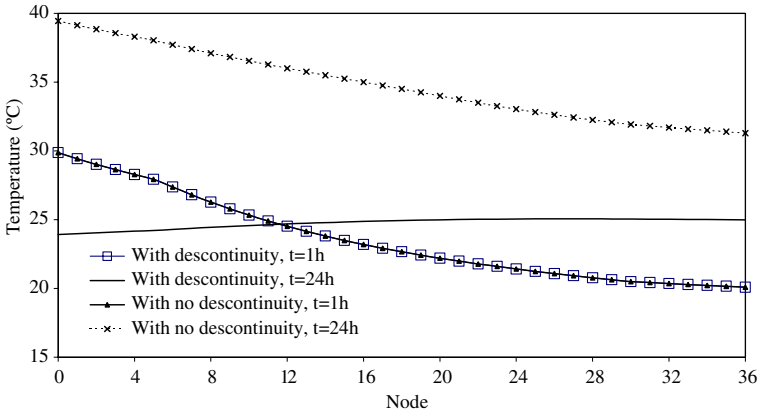

Fig. 14. Temperature profile at 1 h and 24 h under the rain boundary condition.

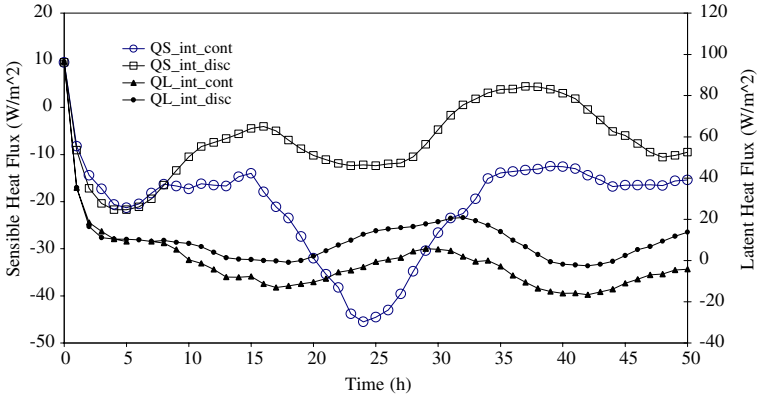

Fig. 15. Sensible and latent heat fluxes under the rain boundary condition.

In Figs. 13 and 14 great differences can be noticed on the moisture content and temperature profiles due, mainly, to the following two aspects: (i) a much higher evaporation rate takes place at the outside surface of the wall and (ii) the phase change term on the energy conservation equation becomes dominant at the interface between the lime mortar and brick layers.

It is noticed, especially in Figs. 13 and 14 with very high moisture content gradients, that the present method is numerically robust and can perform calculations in a very quick and stable fashion.

Fig. 15 shows the sensible and the latent heat fluxes considering the external surface fully saturated of water. It is noticed a significant difference when the discontinuity in the moisture content profile is ignored.

6. Conclusions

The model presented for predicting heat and moisture transfer through porous walls does not take into account convection and radiation heat transfer in the pores, neither the sensible heat transferred by the liquid phase. After all, these simplifying assumptions are generally well accepted in building science.

Thereupon, it was noticed that the presented formulation represents an important contribution to the area of combined heat and moisture transfer through physical domains formed by two or more hygroscopically dissimilar materials. Furthermore, the presented formulation can be easily applied to computer programs of heat and moisture transfer calculation, including just one more equation at each interface without modifying the Philip and De Vries [1] model.

Moreover, there are advantages in using moisture-content based models rather than capillary-pressure or relative-humidity based models due to the fact that hysteresis effects can be less evident on transport coefficients associated to moisture content gradients. In this way, the disregard of hysteresis implies likely small errors when moisture content gradient is the driving force.

The simulations carried out in building elements have shown that the difference - due to the moisture content profile discontinuity at the interface - might bring considerable changes on the calculated values for moisture content and temperature distributions, especially when extreme conditions are used such as the Dirichlet condition for simulating rain effects that produce high gradients of moisture content. Actually, the higher the capillary pressure potential the higher the difference.

Furthermore, it was remarked a very high computational performance and numerical stability for the presented model based only on temperature and moisture content gradients with the MultiTriDiagonal-Matrix Algorithm (MTDMA), which provided numerical stability for all simulations carried out using time steps as high as 1 h, even under the presence of high moisture content and temperature gradients.

Acknowledgments

The authors thank the Brazilian Research Council (CNPq) of the Secretary for Science and Technology of Brazil and Araucária Foundation for support of this work.

References

[1] J.R. Philip, D.A. De Vries, Moisture movement in porous materials under temperature gradients, Trans. Am. Geophys. Union 38 (2) (1957) 222–232.
[2] C.R. Pedersen, Prediction of moisture transfer in building constructions, Build. Environ. (3) (1992) 387–397.
[3] H.M. Künzel, Simultaneous Heat and Moisture Transport in Building Components: One- and Two-dimensional

Calculation Using Simple Parameters, IRB Verlag, Stuttgart, 1995.
[4] P.C.D. Milly, The coupled transport of water and heat in a vertical soil column under atmospheric excitation, Ph.D. Thesis, Massachusetts Institute of Technology, Massachusetts, 1980.
[5] H. Janssen, J. Carmeliet, H. Hens, The influence of soil moisture in the unsaturated zone on the heat loss from buildings via the ground, J. Therm. Envelope Build. Sci. 25 (4) (2002) 275–298.
[6] N. Mendes, I. Ridley, R. Lamberts, P.C. Philppi, K. Budag, UMIDUS: a PC program for the prediction of heat and moisture transfer in porous building elements, in: Proceedings of the Sixth International IBPSA Conference, Building Simulation 1999, Kyoto, Japan, 1999, pp. 277–283.
[7] D.M. Burch, An analysis of moisture accumulation in walls subjected to hot and humid climates, ASHRAE Trans., DE-93-16-4, 1993.
[8] V.P. Freitas, V. Abrantes, P. Crausse, Moisture migration in building walls—analysis of the interface phenomena, Build. Environ. 31 (2) (1996) 99–108.
[9] X. Qiu, F. Haghighat, K. Kumaran, Moisture transport across imperfect hydraulic contact interfaces between building materials, J. Therm. Envelope Build. Sci. 26 (3) (2003) 213–236.
[10] N. Mendes, P.C. Philippi, MultiTriDiagonal-Matrix algorithm for coupled heat transfer in porous media: stability analysis and computational performance, J. Porous Media 7 (3) (2004).
[11] S. Patankar, Numerical Heat Transfer and Fluid Flow, Hemisphere Publishing Corp., New York, 1980.
[12] N. Mendes, P.C. Philippi, Biot number effects on the numerical stability of heat and mass transfer problems, in: Proceedings of the XVIII International Mechanical Engineering Conference (COBEM), São Paulo, Brazil, 2003.
[13] N. Mendes, P.C. Philippi, R. Lamberts, A new mathematical method to solve highly-coupled equations of heat and mass transfer in porous media, Int. J. Heat Mass Transfer 45 (3) (2002) 509–518.
[14] B. Perrin, Etude des transferts couplés de chaleur et de masse dans des matériaux poreux consolidés non saturés utilisés en génie civil, Thèse Docteur d'Etat, Université Paul Sabatier de Toulouse, Toulouse, France, 1985.
[15] N. Mendes, F.C. Winkelmann, R. Lamberts, P.C. Philippi, Moisture effects on conduction loads, Energy Build. 35 (7) (2003) 631–644.
[16] G.H. Santos, N. Mendes, The Solum program for predicting temperature profiles in soils: mathematical models and boundary conditions analyzes, in: Proceedings of the Eighth International IBPSA Conference, Building Simulation 2003, Eindhoven, The Netherlands, 2003.